Valence bond phases of herbertsmithite and related copper kagome materials

M. R. Norman,[1] N. J. Laurita,[2,3] and D. Hsieh[2,3]

[1] *Materials Science Division, Argonne National Laboratory, Argonne, IL 60439, USA*
[2] *Department of Physics, California Institute of Technology, Pasadena, CA 91125, USA*
[3] *Institute for Quantum Information and Matter, California Institute of Technology, Pasadena, CA 91125, USA*

(Dated: November 1, 2019)

Recent evidence from magnetic torque, electron spin resonance, and second harmonic generation indicate that the prototypical quantum spin liquid candidate, herbertsmithite, has a symmetry lower than its x-ray refined trigonal space group. Here, we consider known and possible distortions of this mineral class, along with related copper kagome oxides and fluorides, relate these to possible valence bond patterns, and comment on their relevance to the physics of these interesting materials.

The nature of the ground state of the near neighbor antiferromagnetic Heisenberg model on a kagome lattice (KAHM) has proven to be a challenging problem. Numerical simulations indicate that a variety of different states have comparable energies, including gapped spin liquids, gapless spin liquids, and valence bond solids. This is reflected in the energy spectrum of clusters from exact diagonalization studies, which shows a dense array of excited states extending down to zero energy [1]. In real materials, further richness emerges due to the presence of anisotropic interactions, such as Dzyaloshinskii-Moriya, as well as longer-range exchange. In this context, the lack of observation of an ordered ground state down to 20 mK in herbertsmithite, $ZnCu_3(OH)_6Cl_2$, a mineral where copper ions sit on a perfect kagome lattice, has been a significant result [2–4].

In reality, though, herbertsmithite is far from perfect. Single crystals typically contain 15% of copper ions sitting on interlayer sites nominally occupied by zinc [5]. Moreover, despite x-ray refinements of the crystal structure which indicate perfect trigonal symmetry ($R\bar{3}m$), magnetic torque and electron spin resonance (ESR) [6] find a breaking of the three-fold trigonal axis. This has been recently amplified by second harmonic generation (SHG) data, which is consistent with a monoclinic space group that breaks inversion [7].

To put these results in context, it is first helpful to review known distortions in this mineral class, as well as related materials. The $Cu_4(OH)_6Cl_2$ polymorph from which herbertsmithite arises via Zn substitution for Cu, $Zn_xCu_{4-x}(OH)_6Cl_2$, is clinoatacamite with a monoclinic $P2_1/n$ space group [8]. Upon Zn doping, an intermediate $R\bar{3}$ phase (Zn-paratacamite) is stabilized between $R\bar{3}m$ at high temperatures and $P2_1/n$ at low temperatures. Eventually, the $P2_1/n$ phase disappears, and then for x beyond about 0.34, so does the $R\bar{3}$ phase [9]. For Mg-paratacamite, the $R\bar{3}$ phase has been detected up to x=0.62 [10]. To understand the nature of these two structural phases, we employ the crystallographic tools AMPLIMODES [11] and ISODISTORT [12].

The $R\bar{3}$ phase is driven by an F_2^+ distortion mode resulting in a quadrupling of the unit cell in the planar directions. Here, F is equal to $(0,\frac{1}{2},1)$ in hexagonal reciprocal lattice units, and is related to the M $(\frac{1}{2},0,0)$ point of the hexagonal zone (the difference from M reflects the ABC stacking of layers in the rhombohedral lattice). The resulting crystallographic distortion from the F_2^+ mode is shown in Fig. 1. Basically, the interlayer sites (which would nominally be occupied by Zn in stoichiometric herbertsmithite) divide into two sets, one showing octahedral coordination (1/4 of these sites) and the other a Jahn-Teller distorted 2+2+2 coordination (the remainder). Around the first type, the atoms on the kagome plane rotate about it. This is known as a polar vortex [13] (more formally, an axial toroidal dipole [14]). The distortion pattern around the other interlayer sites has aspects of this as well, but is more complicated. The actual crystal structure is even more complicated, given the presence of F_1^+ and Γ_2^+ secondary modes. Analyzing just the copper kagome sites, one finds two crystallographically distinct sites. This leads to a distribution of Cu-Cu kagome distances. The strongest singlet bond (largest Cu-O-Cu bond angle) forms a pinwheel pattern, as shown in Fig. 2, left. This same pattern is seen in copper kagome fluorides such as $Rb_2Cu_3SnF_{12}$ [15]. Such a pinwheel valence bond pattern has been previously discussed in the KAHM literature given its favorable energetics [16]. Note this phase differs subtly from the so-called diamond valence bond solid, as resonances around diamonds would take one outside of the ground state manifold [17] since those other bonds are not equivalent to the strong bonds. The energy cost for a diamond resonance can be estimated as $2(2J_{12}\text{-}J_{11}\text{-}J_{22})$ where J_{12} is the superexchange of the strong bond and 1,2 refer to the two crystallographically distinct kagome sites. For a resonance around a pinwheel, the energy cost is $6(J_{12}\text{-}J'_{12})$ where J'_{12} refers to the 1-2 bond with the smaller Cu-O-Cu bond angle. Assuming a linear relation of J with the Cu-O-Cu bond angle [18], the estimated cost of a diamond resonance is $0.54J_{12}$ and a pinwheel resonance $1.45J_{12}$ for x=0.29 [9]. These differences become much smaller as x increases (for Mg-paratacamite at x=0.62, they become $0.03J_{12}$ and $0.02J_{12}$, respectively

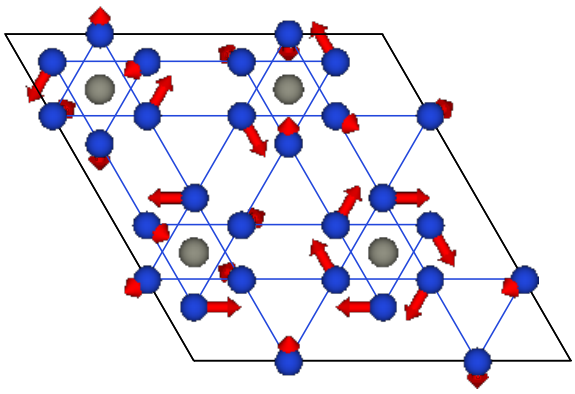

FIG. 1. F_2^+ distortion mode for the R$\bar{3}$ phase of Zn-paratacamite [9] from AMPLIMODES [11] plotted using VESTA [37]. Only the copper/zinc ions are shown in an intersite plane and the two kagome planes that sandwich it (blue kagome, gray intersite). Note the vortex like motion of the kagome coppers about one of the intersites (shared as well by the oxygen, hydrogen and chlorine ions).

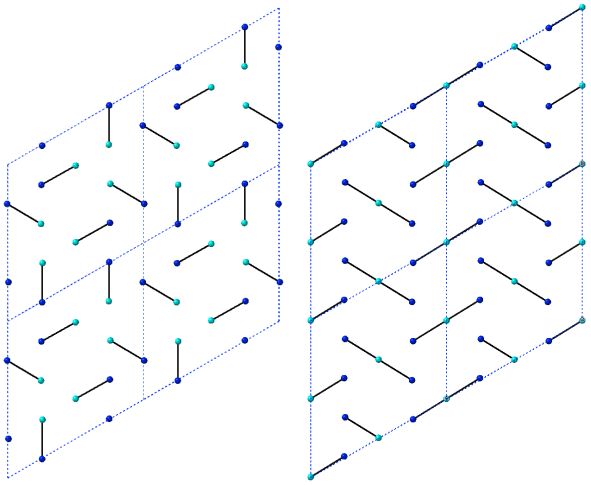

FIG. 2. Valence bond patterns for left: the R$\bar{3}$ phase (Zn-paratacamite) and right: the P2_1/n phase (clinoatacamite). Similar patterns are seen for the P6_3/m and Pnma phases of barlowite, respectively. Only the copper ions are shown in a single kagome plane (the two crystallographically distinct sites are in blue and cyan).

[10]).

The related P2_1/n phase seen in clinoatacamite also arises from an F_2^+ distortion mode, the difference being due to different secondary modes (Γ_3^+ only for P2_1/n). The change in the overall distortion pattern leads to the strong bond now having a herringbone-like structure (Fig. 2, right). This has previously been commented on in regards to the Pnma distortion seen in the closely related material, barlowite, $Cu_4(OH)_6BrF$ [19]. The distortion in the latter case is an M_2^+ mode due to the difference in stacking (AA), the high symmetry phase being hexagonal (P6_3/mmc). In fact, there is a close analogy between the phase transitions seen in weakly Zn doped clinoatacamite (R$\bar{3}$m to R$\bar{3}$ to P2_1/n) and barlowite (P6_3/mmc to P6_3/m to Pnma). In the former case, the primary distortion mode is F_2^+ with secondary modes F_1^+ and Γ_2^+ (R$\bar{3}$) and Γ_3^+ (P2_1/n). For the latter, the primary distortion mode is M_2^+ with secondary modes M_1^+ and Γ_2^+ (P6_3/m) and Γ_5^+ (Pnma). These differences again are due to ABC stacking (rhombohedral) versus AA stacking (hexagonal). This is summarized in Table I.

The detailed temperature dependence of these distortions has been considered by Malcherek *et al.* for clinoatacamite [20] and Welch *et al.* for Zn-paratacamite [9]. The resulting analysis from AMPLIMODES is shown in Fig. 3. Despite the expected first-order nature of the R$\bar{3}$ to P2_1/n phase transition, one sees that the F_2^+ distortion amplitude goes smoothly through the transition, and to a good approximation follows a Landau mean-field behavior of $\sqrt{T_{s1}-T}$ where T_{s1} is the upper transition. Given the limited data, it is hard to quantify the T dependence of the secondary modes. Nominally, the amplitude of the Γ_3^+ mode should be quadratic in F_2^+, but in reality it sets in discontinuously at T_{s2} (lower transition) due to the finite value of F_2^+ at T_{s2}.

TABLE I. Known valence bond solid (VBS) patterns in copper kagome materials. low T is the low temperature crystal structure, high T the high temperature one. mode is the primary distortion mode. z indicates the net buckling of the copper ions in the kagome plane along the hexagonal c-axis (in $\AA$). The high T phase of $Cs_2Cu_3CeF_{12}$ is unknown and so was determined from group-subgroup relations. Note the large buckling often present in the copper fluorides as compared to the copper hydroxychlorides. References are clinoatacamite [20], paratacamite [9], barlowite [19], averievite [25], $Cs_2Cu_3CeF_{12}$ [33], $Cs_2Cu_3ZrF_{12}$ [34], $Cs_2Cu_3SnF_{12}$ [35] and $Rb_2Cu_3SnF_{12}$ [36].

low T	high T	VBS	material	mode	z
P2_1/n	R$\bar{3}$m	herringbone	clinoatacamite	F_2^+	0.07
			$Cs_2Cu_3SnF_{12}$		0.07
P2_1/c	P$\bar{3}$m1	herringbone	averievite	M_2^+	0.00
Pnma	P6_3/mmc	herringbone	barlowite (1)	M_2^+	0.07
R$\bar{3}$	R$\bar{3}$m	pinwheel	paratacamite	F_2^+	0.06
			$Rb_2Cu_3SnF_{12}$		0.38
P6_3/m	P6_3/mmc	pinwheel	barlowite (2)	M_2^+	0.06
P2_1/m	R$\bar{3}$m	zig-zag	$Cs_2Cu_3ZrF_{12}$	F_2^-	0.73
Pnnm	P6_3/mmc	stripe	$Cs_2Cu_3CeF_{12}$	M_3^+	3.93

Returning to the valence bond patterns, a pinwheel pattern is also found in the higher symmetry (P6_3/m) version of barlowite [19] (consistent with the above discussed analogy with Zn-paratacamite) as also listed in Table I. The known list of patterns can be expanded by considering other materials in the class $A_2Cu_3BF_{12}$ where A is an alkali metal and B a 4+ cation [21].

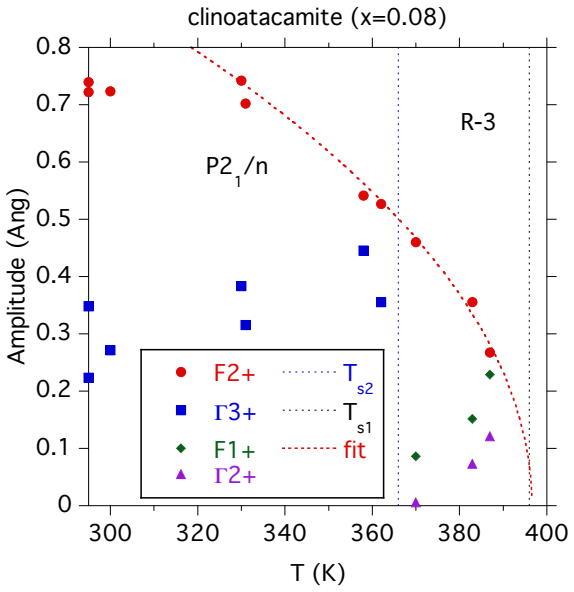

FIG. 3. Temperature dependence of the mode amplitudes (in Å) from clinoatacamite [20] generated by AMPLIMODES [11]. The red dashed curve is a Landau mean-field fit to the F_2^+ mode.

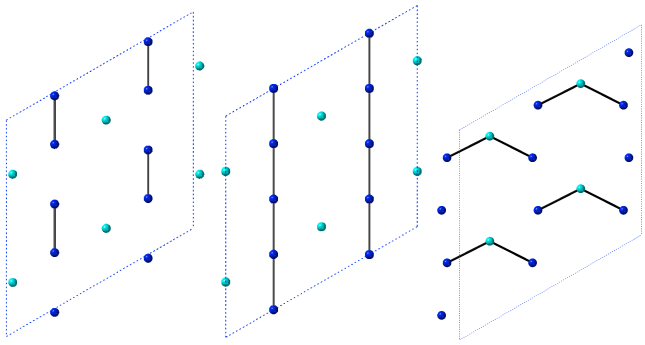

FIG. 4. Various Cm and C2 VBS patterns from a zone-centered mode (Γ_3^-) generated by ISODISTORT [12]. Left: Cm B_{u1} pattern, Middle: Cm B_{u2} pattern, Right: C2 A_u pattern. Here, A_u and B_u refer to point group symmetries of the copper kagome ions. The Cm A_u pattern (not shown) is similar to the Cm B_{u1} one. These patterns are based on just copper kagome ion displacements and the shortest Cu-Cu bonds (only the copper ions are shown in a single kagome plane; the two crystallographically distinct sites are in blue and cyan). The actual pattern will depend on the Cu-O-Cu bond angles once oxygen ion displacements are accounted for.

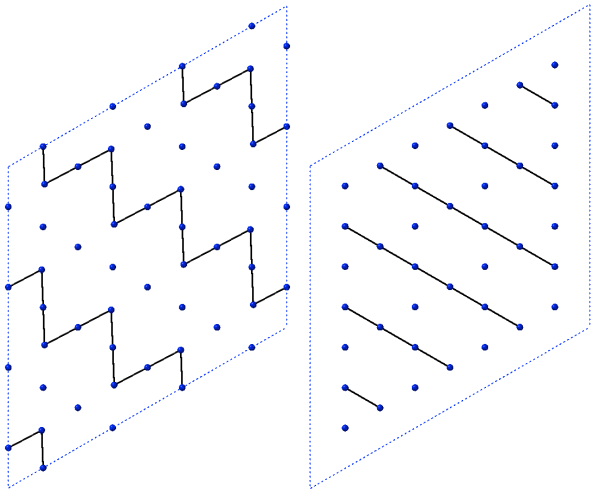

FIG. 5. Two of the Cm VBS patterns from a zone-boundary mode (F_2^-) generated by ISODISTORT [12]. Left: one of the two B_{u1} patterns, Right: one of the two B_{u2} patterns. The other two patterns are dimer patterns similar to Fig. 4a. These patterns are based on just copper kagome ion displacements and the shortest Cu-Cu bonds (only the copper ions are shown in a single kagome plane; there are seven crystallographically distinct sites). The actual pattern will depend on the Cu-O-Cu bond angles once oxygen ion displacements are accounted for.

These are also listed in Table I. In particular, one also finds stripe phases ($Cs_2Cu_3CeF_{12}$) and zig-zag phases ($Cs_2Cu_3ZrF_{12}$). In all cases in Table I, though, inversion symmetry is preserved.

This brings us to the SHG data on herbertsmithite [7]. They indicate a point group of either 2 or m. A likely candidate, then, for the inversion-breaking space group is either Cm or C2. There are two ways this can happen. First, by condensing a zone-centered polar mode (Γ_3^-). Possible valence bond patterns are shown in Fig. 4. Or, by condensing an F_2^- mode as shown in Fig. 5 (note, though, that the F_2^- example given in Table I preserves inversion). Again, these can take the form of stripes or zig-zags, some of which result from buckled planes. One important difference is that for the zone-centered case, one maintains an odd number of copper ions (per plane) in the unit cell. Therefore, we would anticipate an anisotropic spin liquid in this case rather than a valence bond solid [22]. For the zone-boundary modes, though, the unit cell size increases resulting in an even number of copper ions instead, so this would be a valence bond solid.

One interesting point about the Cm and C2 space groups is that they are in general ferroelectric, with the polar axis along the 2-fold (hexagonal b axis) for C2, and perpendicular to this axis for Cm. Ferroelectric behavior has been claimed for the cobalt analog of clinoatacamite, with a proposed structural distortion of R3m [23]. Indications of ferroelectric-like behavior has also been seen in averievite [24], where a transition from the intermediate $P2_1/c$ phase to a lower temperature phase of unknown symmetry has been observed [25]. This brings up the question of spin-lattice coupling. The SHG signal in herbertsmithite follows the predicted temperature dependence of the spin-spin correlator for a kagome lattice [7]. This is consistent with the temperature dependence of phonon linewidths [26]. The idea here is that

the superexchange J is sensitive to distortions given its dependence on the Cu-O-Cu bond angle, harking back to early work by Baltensperger [27]. Spin-lattice couplings have been quantified in clinoatacamite using Raman data [28]. Ultimately, they can lead to multiferroic behavior, as observed in the distorted kagome material $KCu_3As_2O_7(OH)_3$ [29].

Finally, what does all of this have to do with the KAHM? Density matrix renormalization group simulations have indicated that the ground state is a melted version of a twelve-site diamond valence bond solid, closely related to the pinwheel pattern [30]. This has been further investigated by more recent numerical work [31], though related numerical simulations favor a Dirac spin liquid instead [32]. Small perturbations could certainly stabilize a valence bond solid, or an anisotropic spin liquid. Given the above results, such models should be further explored to understand the rich physics of the Heisenberg model on a kagome lattice and its material realizations.

M.R.N. was supported by the Materials Sciences and Engineering Division, Basic Energy Sciences, Office of Science, U.S. Dept. of Energy. N.J.L. acknowledges partial support from an Institute for Quantum Information and Matter Postdoctoral Fellowship. D.H. acknowledges support from an ARO PECASE award W911NF-17-1-0204.

[1] P. Lecheminant, B. Bernu, C. Lhuillier, L. Pierre and P. Sindzingre, Phys. Rev. B **56**, 2521 (1997).
[2] M. P. Shores, E. A. Nytko, B. M. Bartlett and D. G. Nocera, J. Am. Chem. Soc. **127**, 13462 (2005).
[3] P. Mendels and F. Bert, J. Phys. Soc. Japan **79**, 011001 (2010).
[4] M. R. Norman, Rev. Mod. Phys. **88**, 041002 (2016).
[5] T. H. Han, J. S. Helton, S. Chu, A. Prodi, D. K. Singh, C. Mazzoli, P. Muller, D. G. Nocera and Y. S. Lee, Phys. Rev. B **83**, 100402 (2011).
[6] A. Zorko, M. Herak, M. Gomilsek, J. van Tol, M. Velazquez, P. Khuntia, F. Bert and P. Mendels, Phys. Rev. Lett. **118**, 017202 (2017).
[7] N. J. Laurita, A. Ron, J. W. Han, A. Scheie, J. P. Sheckelton, R. W. Smaha, W. He, J.-J. Wen, J. S. Lee, Y. S. Lee, M. R. Norman and D. Hsieh, arXiv:1910.13606.
[8] J. D. Grice, J. T. Szymanski and J. L. Jambor, Can. Mineral. **34**, 73 (1996).
[9] M. D. Welch, M. J. Sciberras, P. A. Williams, P. Leverett, J. Schluter and T. Malcharek, Phys. Chem. Minerals **41**, 33 (2014).
[10] A. R. Kampf, M. J. Sciberras, P. Leverett, P. A. Williams, T. Malcherek, J. Schluter, M. D. Welch, M. Dini and A. A. M. Donoso, Mineral. Mag. **77**, 3113 (2013).
[11] D. Orobengoa, C. Capillas, M. I. Aroyo and J. M. Perez-Mato, J. Appl. Cryst. **42**, 820 (2009).
[12] B. J. Campbell, H. T. Stokes, D. E. Tanner and D. M. Hatch, J. Appl. Cryst. **39**, 607 (2006).
[13] A. K. Yadav, C. T. Nelson, S. L. Hsu, Z. Hong, J. D. Clarkson, C. M. Schlepuetz, A. R. Damodaran, P. Shafer, E. Arenholz, L. R. Dedon, D. Chen, A. Vishwanath, A. M. Minor, L. Q. Chen, J. F. Scott, L. W. Martin and R. Ramesh, Nature **530**, 198 (2016).
[14] V. M. Dubovik, L.A. Tosunyan and V. V. Tugushev, Sov. Phys. JETP **63**, 344 (1986).
[15] K. Matan, T. Ono, Y. Fukumoto, T. J. Sato, J. Yamaura, M. Yano, K. Morita and H. Tanaka, Nature Phys. **6**, 865 (2010).
[16] B.-J. Yang and Y. B. Kim, Phys. Rev. B **79**, 224417 (2009).
[17] A. Wietek and A. M. Lauchli, arXiv:1908.02762 (2019).
[18] V. H. Crawford, H. W. Richardson, J. R. Wasson, D. J. Hodgson and W. E. Hatfield, Inorg. Chem. **15**, 2107 (1976). This linear relation is such that the critical angle (where J=0) is 97.54°.
[19] R. W. Smaha, W. He, J. M. Jiang, C. J. Titus, J. Wen, Y.-F. Jiang, J. P. Sheckelton, S. G. Wang, Y.-S. Chen, S. J. Teat, A. A. Aczel, Y. Zhao, G. Xu, J. W. Lynn, H.-C. Jiang and Y. S. Lee, arXiv:1907.00454 (2019).
[20] T. Malcherek, B. Mihailova and M. D. Welch, Phys. Chem. Minerals **44**, 307 (2017).
[21] K. Matan, T. Ono, G. Gitgeatpong, K. de Roos, P. Miao, S. Torii, T. Kamiyama, A. Miyata, A. Matsuo, K. Kindo, S. Takeyama, Y. Nambu, P. Piyawongwatthana, T. J. Sato and H. Tanaka, Phys. Rev. B **99**, 224404 (2019).
[22] B. K. Clark, J. M. Kinder, E. Neuscamman, G. K.-L. Chan and M. J. Lawler, Phys. Rev. Lett. **111**, 187205 (2013).
[23] X.-L. Xu, D.-D. Meng, X.-G. Zheng, I. Yamauchi, I. Watanabe and Q.-X. Guo, Phys. Rev. B **95**, 024111 (2017).
[24] T. Biesner, A. Pustogow, H. Zheng, J. F. Mitchell and M. Dressel (unpublished).
[25] A. S. Botana, H. Zheng, S. H. Lapidus, J. F. Mitchell and M. R. Norman, Phys. Rev. B **98**, 054421 (2018).
[26] A. B. Sushkov, G. S. Jenkins, T.-H. Han, Y. S. Lee and H. D. Drew, J. Phys.: Condens. Matter **29**, 095802 (2017).
[27] H. Baltensperger and J. S. Helman, Helv. Phys. Acta **41**, 668 (1968).
[28] X.-D. Liu, X.-G. Zheng, D.-D. Meng, X.-L. Xu and Q.-X. Guo, J. Phys.: Condens. Matter **25**, 256003 (2013).
[29] G. J. Nilsen, Y. Okamoto, H. Ishikawa, V. Simonet, C. V. Colin, A. Cano, L. C. Chapon, T. Hansen, H. Mutka and Z. Hiroi, Phys. Rev. B **89**, 140412 (2014).
[30] S. Yan, D. A. Huse and S. R. White, Science **332**, 1173 (2011).
[31] A. Ralko, F. Mila and I. Rousochatzakis, Phys. Rev. B **97**, 104401 (2018).
[32] Y.-C. He, M. P. Zalatel, M. Oshikawa and F. Pollmann, Phys. Rev. X **7**, 031020 (2017).
[33] T. Amemiya, M. Yano, K. Morita, I. Umegaki, T. Ono, H. Tanaka, K. Fujii and H. Uekusa, Phys. Rev. B **80**, 100406 (2009).
[34] S. A. Reisinger, C. C. Tang, S. P. Thompson, F. D. Morrison and P. Lightfoot, Chem. Mater. **23**, 4234 (2011).
[35] L. J. Downie, C. Black, E. I. Ardashnikova, C. C. Tang, A. N. Vasiliev, A. N. Golovanov, P. S. Berdonosov, V. A. Dolgikh and P. Lightfoot, CrystEngComm **16**, 7419 (2014).
[36] L. J. Downie, S. P. Thompson, C. C. Tang, S. Parsons and P. Lightfoot, CrystEngComm **15**, 7426 (2013).
[37] K. Momma and F. Izumi, J. Appl. Cryst. **44**, 1272 (2011).